Preprints.org

Article

Not peer-reviewed version

Experimental Evidence of High Renewable Energy Employing a Symmetric Circuit with a Divergent Current Density

Shinichi Ishiguri *

Posted Date: 27 February 2026

doi: 10.20944/preprints202504.2514.v4

Keywords: applied physics; divergent current density; highly symmetric circuit; quantum mechanics; renewable energy; stray capacitor

Preprints.org is a free multidisciplinary platform providing preprint service that is dedicated to making early versions of research outputs permanently available and citable. Preprints posted at Preprints.org appear in Web of Science, Crossref, Google Scholar, Scilit, Europe PMC.

Copyright: This open access article is published under a Creative Commons CC BY 4.0 license, which permit the free download, distribution, and reuse, provided that the author and preprint are cited in any reuse.

Preprints.org (www.preprints.org) | NOT PEER-REVIEWED | Posted: 27 February 2026 doi:10.20944/preprints202504.2514.v4

Disclaimer/Publisher's Note: The statements, opinions, and data contained in all publications are solely those of the individual author(s) and contributor(s) and not of MDPI and/or the editor(s). MDPI and/or the editor(s) disclaim responsibility for any injury to people or property resulting from any ideas, methods, instructions, or products referred to in the content.

Article

Experimental Evidence of High Renewable Energy Employing a Symmetric Circuit with a Divergent Current Density

Shinichi Ishiguri

Nihon University, 1-2-1 Izumi-Cho, Narashinoshi, Chiba 275-8575, Japan; shinichi.ishiguri@gmail.com;Note that the university was retired by the author.

Abstract

Limited fossil fuels have created a societal energy crisis necessitating the use of renewable energy. However, existing renewable energy sources are problematic and incur high costs. To overcome these issues, we propose a new renewable energy source with a divergent current density and highly symmetric circuits. This circuit comprises two voltage sources and two identical loads that output a few energies. In this circuit, stray capacitors in the vacuum play an important role to generate a divergent current density. This divergent current generates large electric power. This paper verified this fact theoretically and experimentally. In the theory, a simple Hamiltonian of Schrodinger equation results in a unique current–voltage characteristic, allowing for the current to flow along a large load without the Joule heating. During our experiments, a considerably large divergent current flowed into a huge resistance, boosting the output electric power to a level almost equal to that of a nuclear power station. In addition, the experimental results were consistent with the theoretical expectations. In conclusion, this paper has succeeded to present a novel system that generates considerably large energy in the theory and experiments.

Keywords: applied physics; divergent current density; highly symmetric circuit; quantum mechanics; renewable energy; stray capacitor

1. Introduction

The depletion of fossil fuels such as crude oil and natural gas has created societal energy problems. Moreover, the limited availability of high-cost crude oil has caused economic problems. To mitigate these concerns, countries are attempting to introduce renewable energies [1–6], but such alternatives cannot (in most cases) satisfy 100% of the demand. Moreover, most renewable energies fluctuate with natural climate variations, complicating the system, planning, and control methods. The most promising of the existing renewable energies are solar and wind power [7,8] but they require high costs as will be described. Furthermore, fossil fuel consumption is a cause of rising CO_2 concentration [9,10]. The spread of renewable energy sources must be considered from both economic and technological perspectives. Highly efficient, low-cost energy generation is of major importance [11,12].

To reduce the atmospheric CO_2 concentration, existing renewable energy sources such as solar and wind power must be widely adopted. However, the integration of renewable energy into the existing power systems risks frequency and voltage disruptions. Moreover, effective performance from the existing energy sources requires many expensive storage batteries.

Japan has declared a goal of net-zero carbon by 2050, but simulations [13,14] have shown that meeting this goal might be impossible without breakthrough technologies.

© 2025 by the author(s). Distributed under a Creative Commons CC BY license.

Preprints.org (www.preprints.org) | NOT PEER-REVIEWED | Posted: 27 February 2026 doi:10.20944/preprints202504.2514.v4

The main problems with the existing renewable energy and nuclear power generation are summarized below.

1) Renewable energy sources depend on the weather, necessitating large and expensive storage batteries. Moreover, introducing renewable energy sources to the existing energy systems will destabilize the outputs.
2) Simulations assessing the possibility of achieving net-zero carbon in Japan have included nuclear power generation without considering its dangers. For instance, the Fukushima nuclear accident in Japan in 2011 caused extensive damage.
3) Introducing renewable energy incurs high costs in all countries.

To address the abovementioned concerns, this paper proposes a new system for stable energy production meeting the demands of Japan, i.e., the required amount of energy in the right place at the right time. Moreover, our system is highly efficient with low costs.

Our previously proposed energy-generating system [15,16] could not generate sufficiently large amounts of energy, although they could provide stable energies. The present paper proposes a new concept for generating substantial renewable energy using a highly symmetric circuit with significantly low costs. When certain conditions are satisfied, the circuit provides an apparent divergent current with no Joule heating to both paired light-emitting diodes (LEDs) and paired direct current (DC) motors, boosting the electric power. This power generation phenomenon is verified in both theory and experiments. We discuss the good agreement between the theory and experiments, and will describe whether the results satisfy the purpose and motivation of this study. Moreover, there are a few articles relevant to this study that use quantum computing to explore renewable energy or integrate quantum computing and renewable energy (e.g., [17]). Most existing studies conducted only simulations and arrived at conclusions without experimental evidence. The novelty of this study is to realize quantum mechanics-based renewable energy sources in terms of theory and experiment to solve the current energy problem in the world. Consequently, this paper succeeded in presenting a considerably large output energy source with high efficiency, with few costs and no dangerous substances.

2. Materials and Methods

Figure 1 is a schematic of the presented model near its initial state. The circuit employs two same-output voltage sources V and two identical loads which are not pure electrical loads, as they must output an energy of (E_{out}) per electron. As shown in the figure, this circuit system is highly symmetric. The voltage (V) is expressed in terms of the electric potential (φ_e) as follows:

$$V \equiv \varphi_e - (-\varphi_e) = 2\varphi_e. \quad (1)$$

Notably, α, β, α' and β' in Figure 1 are the names of taps.

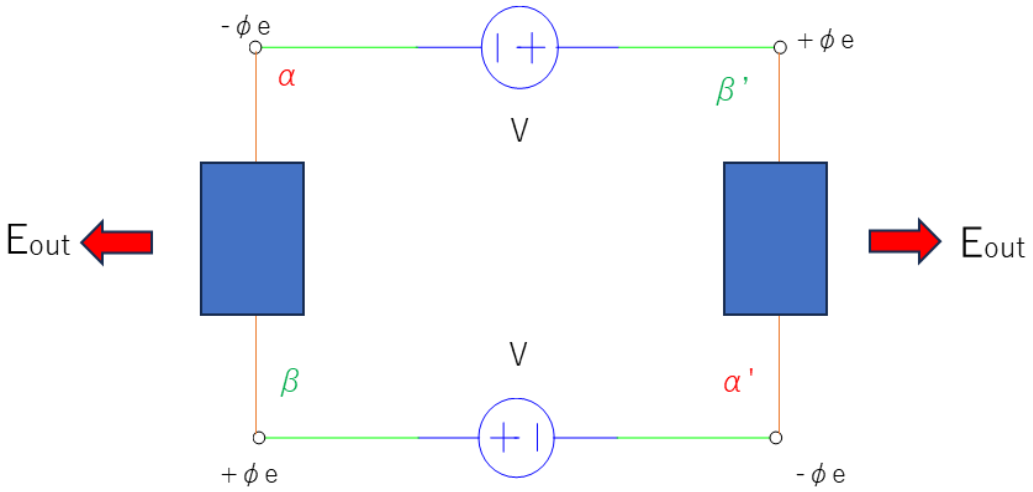

© 2025 by the author(s). Distributed under a Creative Commons CC BY license.

Preprints.org (www.preprints.org) | NOT PEER-REVIEWED | Posted: 27 February 2026 doi:10.20944/preprints202504.2514.v4

Figure 1. Circuit configuration near the initial state, consisting of identical loads (blue blocks) that must output an energy of (E_{out}) per electron. Note that (φ_e) is the electric potential, and then α, β, α', and β' are taps. Moreover, (V) is the output of a voltage source.

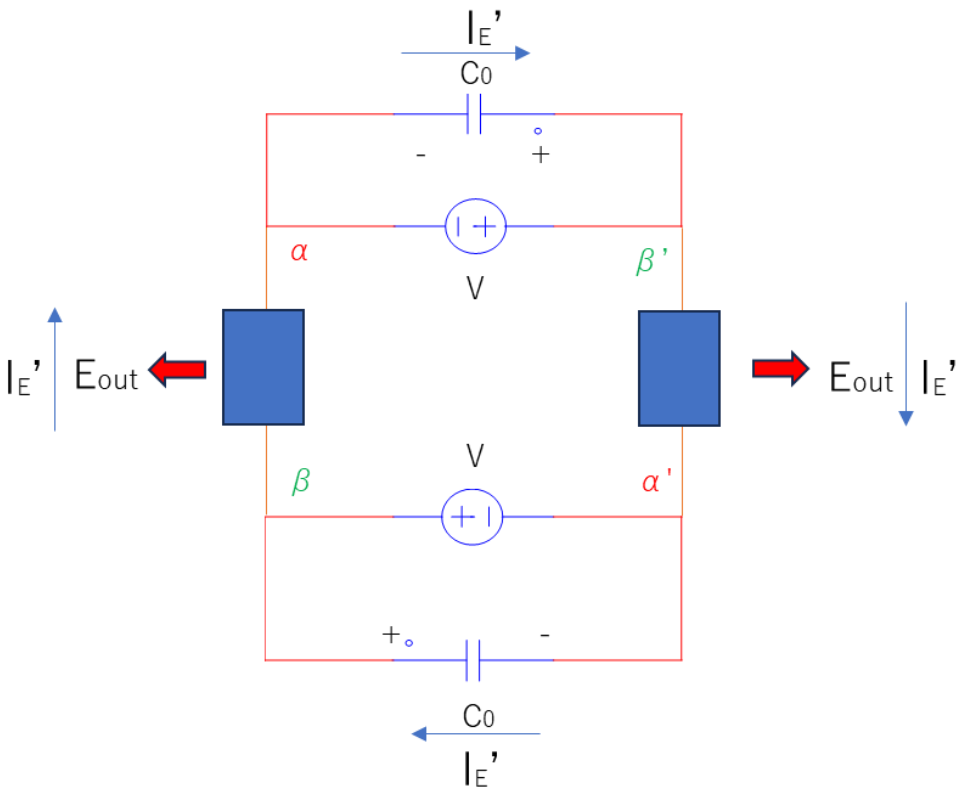

Figure 2. Circuit configuration at the transition time (t_c) with stray capacitors C_0. The paired condensers repetitively store and discharge energy, generating a constant current (I_E'). The voltage sources (V) in this state are dead apart from momentary activity near the initial state. Note that α, β, α', and β' are taps. Moreover, (E_{out}) is the output energy per electron from a load.

The principle of the model is shown in Figure 2, which (unlike Figure 1) includes a pair of stray capacitors C_0 embedded in a vacuum. At initial time $t = 0$, the stray condensers C_0 are shorted. (Note that a condenser is generally shorted at the initial state due to its voltage–current characteristic.) Moreover, completely at $t = 0$, the loads do not output the energies owing to no current because the stray condenser C_0 are shorted; thus, at $t = 0$, all the currents in the system are distributed to the stray condenser C_0. At some transition time $t = t_c$, there is a transient current (i) in the loads and an emergent electric potential (φ) defined as follows:

$$E_{out} = 2e\varphi, \qquad (2)$$

where e is the electron charge.

At time (t_c), for the above definition of the emergent electric potential (φ) to survive, the following condition must be satisfied:

$$\frac{1}{2}C_0(2\varphi)^2 > Ri^2t_c. \qquad (3)$$

The right-hand side of this inequality indirectly defines the energy of the voltage source V, which essentially equates to Joule heating. The resistance (R) is the net one including the loads, lead and contact resistances. Note that if the condition (3) is met, $|\varphi| > |\varphi_e|$ is formed at a tap, implying that the electric potential (φ) is charged at that tap and that instead (φ_e) vanishes. This is originated from the fact that the electric potentials (φ) and (φ_e) cannot coexist at a tap.

For an electron, we can rewrite the condition (3) as

$$|e\varphi| > \frac{1}{2}k_BT, \qquad (4)$$

© 2025 by the author(s). Distributed under a Creative Commons CC BY license.

Preprints.org (www.preprints.org) | NOT PEER-REVIEWED | Posted: 27 February 2026 doi:10.20944/preprints202504.2514.v4

where k_B and T denote the Boltzmann constant and temperature, respectively. Both the sides of inequality (4) imply the average energy of an electron. The left side implies a work which an electron receives from a condenser. In most situations, the temperature is the room temperature (i.e., $T \approx 300\ [K]$) but inequality (4) implies that Joule heating is ineffective.

As discussed later, the term $(e\varphi)$ equals the kinetic energy of an electron.

When the above condition is satisfied, the energies stored in the condensers are discharged, because the energy balance between the condenser C_0 and the voltage source V breaks. Under the energy conservation law, energy interchange between the paired up-condenser and down-condenser in Figure 2 induces a constant current ($I_{E'}$) along the C_0-load-to-C_0-load loop. Because the condensers C_0 are embedded in a vacuum and cannot be touched, a divergent current ($I_{E'}$) is generated. Note that if the inequality is not satisfied, the condensers never discharge their current but if the inequality is satisfied, the voltage sources V momentary operate until the condensers begin discharging at time (t_c) and are dormant thereafter, thereby generating energy.

We now discuss the emergent electric potential (φ) after steady state, $t \geq t_c$. In other words, we discuss how the input electric potential (φ_e) vanishes in the steady state.

In the vicinity of tap α or β at $t = t_c$, we have

$$d\varphi_e \equiv \overrightarrow{E_e} \cdot d\vec{s}, \quad (5)$$

and

$$d\varphi_{c0} \equiv \overrightarrow{E_{c0}} \cdot d\vec{s}, \quad (6)$$

where $\boldsymbol{E}_e$ and $\boldsymbol{E}_{c0}$ denote the ohmic and condenser-associated electric fields, respectively.

Note that the vector (d$\boldsymbol{s}$) aligns along the direction of ($I_{E'}$).

Given that the condenser discharges the current at this time, we have:

$$d\varphi_{c0} = -E_{c0} ds. \quad (7)$$

Moreover,

$$d\varphi_e = E_e ds. \quad (8)$$

However, in the vicinity of a tap, because $\varphi_e = \varphi_{c0}$, we have:

$$d\varphi_e = d\varphi_{c0}, \quad (9)$$

giving rise to

$$E_e = E_{c0} = 0. \quad (10)$$

This equation implies that the ohmic voltage is ineffective. Moreover, considering that a voltage is derived by the definite integral or circular integral of an electric field, the input electric potential (φ_e) is zero. The voltage of the condenser is updated because of the existence of the left energy of the condition (3).

© 2025 by the author(s). Distributed under a Creative Commons CC BY license.

Preprints.org (www.preprints.org) | NOT PEER-REVIEWED | Posted: 27 February 2026 doi:10.20944/preprints202504.2514.v4

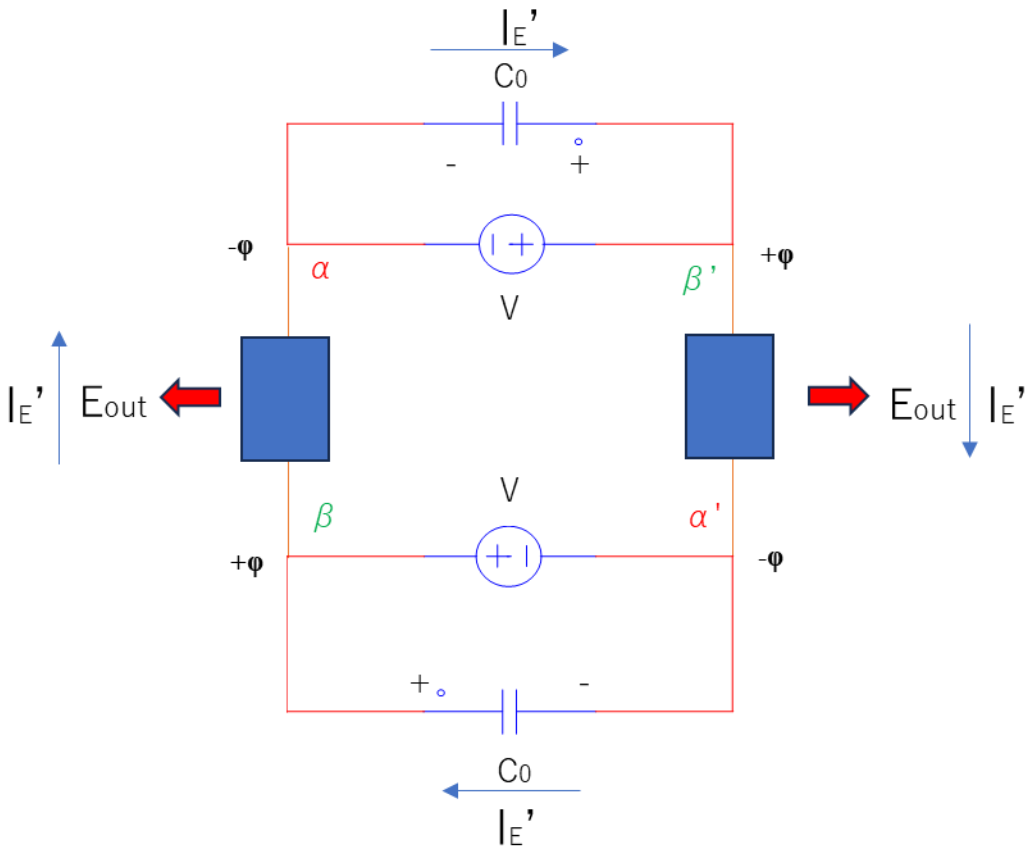

Figure 3. Circuit configuration showing the distribution of the emergent electric potential (φ) associated with the output energy (E_{out}). The voltage sources $V = 2\varphi_e$ steadily decay.

The electric potential is defined as

$$2e\varphi \equiv E_{out}, \quad (11)$$

with

$$|\varphi| > |\varphi_e|. \quad (12)$$

This emergent electric potential (φ) is demonstrated in Figure 3. The electric potential (φ) is not ohmic but a new electric potential of the stray condenser during time $t \geq t_c$

Let us introduce wave function contributing to the electron motion.

The general form of the Hamiltonian is

$$H_{total} \equiv H_G + H_{eff}, \quad (13)$$

where the first and second terms describe the center-of-mass motion and the net interaction energies, respectively. As will be discussed soon, the following assumption holds:

$$H_G \gg H_{eff}. \quad (14)$$

Assuming that the scalar $|e\varphi|$ is distributed along the x-axis and provides a center-of-mass motion equal to the kinetic energy, this scalar results in a relatively large kinetic energy, as will be described. Thus, the rest of the momenta along the other dimensions can be neglected. The term $|e\varphi|$ provides a center-of-mass motion because it is a constant that does not depend on relative ordinates. Therefore, one-dimension motion is possible. Next, let us consider the reason for the formation of the approximation in Eq. (14), i.e., why (H_{eff}) is neglected. We can assume a uniform electrical potential (φ) at tap α or β, implying that each electron has approximately the same electrical potential (φ) because whether the potential (φ) is macroscopic or microscopic cannot be discerned. Considerably, as (φ) cannot coexist with a Coulomb interaction potential (φ_M), the Hamiltonian (H_{eff}) is sufficiently small. Note that the satisfaction of the condition described in Eq. (4) implies that there is no heating energy in a local position; thus, we do not need to consider the interaction of many electrons. In other

© 2025 by the author(s). Distributed under a Creative Commons CC BY license.

Preprints.org (www.preprints.org) | NOT PEER-REVIEWED | Posted: 27 February 2026 doi:10.20944/preprints202504.2514.v4

words, a one-particle picture (i.e., no many-body interaction) is allowed. Moreover, the condition described in Eq. (4) implies that an electron penetrates lattices. Thus, an electron receives no external forces from the lattices.

The Hamiltonians at tap α are

$$-\frac{\hbar^2}{2m}\frac{d^2}{dx^2}+(+e\varphi)\equiv H_{\alpha\uparrow}+H_{\alpha\downarrow}, \quad (15)$$

here m, $H_{\alpha\uparrow}$, and $H_{\alpha\downarrow}$ denote the electron mass, Hamiltonian of the up-spin electron, and Hamiltonian of the down-spin electron, respectively. Because of symmetry, the Hamiltonians of tap α' take the same forms as those of tap α (Eq. (15)). Moreover, each Hamiltonian essentially implies a one-particle picture.

The exclusion principle states that the energies of up- and down-spin electrons are the same. Therefore, we now consider degeneracies.

$$\frac{\hbar^2k_\alpha^2}{2m}\equiv|+e\varphi|, \quad (16)$$

where k is the wavenumber.

Thus,

$$k_\alpha=\pm\frac{\sqrt{2me\varphi}}{\hbar}. \quad (17)$$

Thus, the wave functions with each spin are

$$\psi_{\alpha\uparrow}=|\psi|\exp\left(j\frac{\sqrt{2me\varphi}}{\hbar}x\right) \text{ and } \psi_{\alpha\downarrow}=\delta(x). \quad (18)$$

Note that we employed a delta function as the eigenfunction of the position.

For the case of tap α' we alter the correspondence of the first and second terms of Eq. (15).

$$\psi_{\alpha'\downarrow}=|\psi|\exp\left(-j\frac{\sqrt{2me\varphi}}{\hbar}x\right) \text{ and } \psi_{\alpha'\uparrow}=\delta(x). \quad (19)$$

Note that (j) is the imaginary unit. Similar to tap α, tap β satisfies the following Hamiltonians:

$$-\frac{\hbar^2}{2m}\frac{d^2}{dx^2}+(-e\varphi)\equiv H_{\beta\downarrow}+H_{\beta\uparrow}. \quad (20)$$

From the exclusion principle,

$$\frac{\hbar^2k_\beta^2}{2m}\equiv|-e\varphi|, \quad (21)$$

where

$$k_\beta=\mp\frac{\sqrt{2me\varphi}}{\hbar}. \quad (22)$$

The wave functions of β are

$$\psi_{\beta\downarrow}=|\psi|\exp\left(j\frac{\sqrt{2me\varphi}}{\hbar}x\right) \text{ and } \psi_{\beta\uparrow}=\delta(x-a). \quad (23)$$

Note that the origin of the delta function was distinguished from Eqs. (18) and (19).

For the case of tap β', we alter the correspondence of the first and second terms of Eq. (20):

$$\psi_{\beta'\uparrow}=|\psi|\exp\left(-j\frac{\sqrt{2me\varphi}}{\hbar}x\right) \text{ and } \psi_{\beta'\downarrow}=\delta(x-a). \quad (24)$$

The Slater determinant:

$$\psi_E\equiv\left(\psi_{\alpha\uparrow}\psi_{\beta\downarrow}-\psi_{\alpha\downarrow}\psi_{\beta\uparrow}\right)+\left(\psi_{\alpha'\uparrow}\psi_{\beta'\downarrow}-\psi_{\alpha'\downarrow}\psi_{\beta'\uparrow}\right). \quad (25)$$

In the above equation, the delta functions are substituted.

$$\psi_E=\left(\psi_{\alpha\uparrow}\psi_{\beta\downarrow}-\psi_{\alpha'\downarrow}\psi_{\beta'\uparrow}\right). \quad (26)$$

Thus,

$$\psi_E=|\psi|^2\{\exp\left(j\frac{2\sqrt{2me\varphi}}{\hbar}x\right)-\exp\left(-j\frac{2\sqrt{2me\varphi}}{\hbar}x\right)\}. \quad (27)$$

The first and second terms of the above equation correspond to the left- and right-sides of the circuit in Figure 3, respectively. Note that the normalization of the wavefunction ψ_E is not considered here. Instead, a normalization of each term wavefunction is now considered. Each term wavefunction of this equation implies a divergent current density and thus the first and second terms of Eq. (27) are basically independent.

Therefore, for symmetry, we consider only the first term of Eq. (27).

© 2025 by the author(s). Distributed under a Creative Commons CC BY license.

Preprints.org (www.preprints.org) | NOT PEER-REVIEWED | Posted: 27 February 2026 doi:10.20944/preprints202504.2514.v4

The uncertainty relation gives

$\Delta p_e \Delta x = \frac{1}{2}\hbar$.

Because the momentum (p_e) is constant as ($\hbar k$), the uncertainty (Δx) becomes infinite, defying the classical physical motion of an electron from one tap to the other. The wavefunction of the left part of the circuit is:

$$\psi_L \equiv |\psi_L| \exp\left[j \frac{2\sqrt{2me\varphi}}{\hbar} x\right]. \quad (28)$$

The probability density (j_E) of the flow:

$$j_E = \frac{\hbar}{2mj}\left(\psi_L^* \frac{d\psi_L}{dx} - \psi_L \frac{d\psi_L^*}{dx}\right) \quad (29)$$

is solved as

$$j_E = \frac{\hbar}{2m} \frac{4\sqrt{2me\varphi}}{\hbar} |\psi_L|^2. \quad (30)$$

Herein, we separately consider paired LEDs or paired DC motors as the loads to calculate $|\psi_L|^2$

1) *DC-motor loads*

From the normalization condition:

$$\int |\psi_L|^2 dv \equiv 1, \quad (31)$$

we have

$$|\psi_L|^2 \lambda^3 = 1, \quad (32)$$

where λ is the wavelength of an electron.

The wavenumber (k) is defined as

$$k \equiv \frac{1}{\lambda}. \quad (33)$$

Thus,

$$|\psi_L|^2 \approx k^3. \quad (34)$$

The wavenumber is also derived as

$$k = \frac{2\sqrt{2me\varphi}}{\hbar}, \quad (35)$$

from which the flow probability density (j_E) is obtained as

$$j_E = \frac{4\sqrt{2me\varphi}}{2m}\left(\frac{2\sqrt{2me\varphi}}{\hbar}\right)^3. \quad (36)$$

That is,

$$j_E = \frac{64m^2e^2}{m\hbar^3}\varphi^2. \quad (37)$$

To obtain the net current density [A/m²], we multiply Eq. (37) by the electronic charge (e):

$$j'_E = \frac{64me^3}{\hbar^3}\varphi^2 \approx 2 \times 10^{17}\varphi^2. \quad (38)$$

Here, the area (S_i) is considered as a unit cell; for example,

$$S_i \cong (1.5 \times 10^{-9})^2 \ [\text{m}^2]. \quad (39)$$

Importantly, the net observed current (I'_E) is then derived as

$$I'_E \approx 0.45\varphi^2 \ [\text{A}]. \quad (40)$$

2) *LED loads*

Under the normalization condition:

$$\int |\psi_L|^2 dv \equiv 1, \quad (41)$$

© 2025 by the author(s). Distributed under a Creative Commons CC BY license.

Preprints.org (www.preprints.org) | NOT PEER-REVIEWED | Posted: 27 February 2026 doi:10.20944/preprints202504.2514.v4

we again have:

$$|\psi_L|^2\lambda^3 = 1, \tag{42}$$

but here we consider the momentum (k_L) of a photon with wavenumber [18]:

$$k_L = \frac{2\pi}{\lambda}. \tag{43}$$

The photon imparts its momentum to an electron and hole and thus the wave number of a carrier becomes a half of Eq. (43), considering the conservation of the momentum.

$$|\psi_L|^2 = \frac{1}{\pi^3}k^3 \tag{44}$$

and

$$j_E = \frac{4\sqrt{2me\varphi}}{2m}\left(\frac{2\sqrt{2me\varphi}}{\hbar}\right)^3\frac{1}{\pi^3} = \frac{64m^2e^2}{m\hbar^3}\frac{1}{\pi^3}\varphi^2. \tag{45}$$

Similar to the DC motor, the LED loads obtain a net current density of:

$$j_E' = \frac{64me^3}{\hbar^3}\frac{1}{\pi^3}\varphi^2 \approx 6.4\times10^{15}\varphi^2 \ \text{[A/m}^2\text{]}. \tag{46}$$

As the net current is contributed by an electron and a hole, we have:

$$j_{E,net}' \approx 2\times j_E' = 1.3\times10^{16}\varphi^2 \ \text{[A/m}^2\text{]}. \tag{47}$$

Within the area (S_i) of a unit cell, e.g.,

$$S_i \cong (1.8\times10^{-9})^2 \ \text{[m}^2\text{]}, \tag{48}$$

the net current is

$$I_E' \approx 0.04\varphi^2\text{[A]}. \tag{49}$$

Next, the DC-motor loads must satisfy two conditions. Let us consider these conditions:

The general motion equation of a motor is [19] as follows:

$$V_a = R_aI_a + L\frac{dI_a}{dt} + E, \tag{50}$$

where R_a [Ω], I_a [A], L [H], and E [V] denote the inner resistance, working current, inductance, and reverse electromotive force, respectively.

Let us first obtain the general solution from Eq. (50). This general solution is immediately obtained as

$$I_a = I_a(0)\exp(-\frac{R_a}{L}t). \tag{51}$$

At completely $t = 0$ when all currents flow into the stray condensers C_0 in our system, the initial current in the motor is zero; that is,

$$I_a(0) \equiv 0. \tag{52}$$

Moreover, the special solution of Eq. (50) is derived by

$$I_a \equiv A = const.. \tag{53}$$

Thus, by the substitution to Eq. (50), the special solution becomes

$$A = \frac{V_a - E}{R_a}, \tag{54}$$

and thus, the net solution, i.e., the sum of the general solution and the special solution, is

$$I_a = I_a(0)\exp\left(-\frac{R_a}{L}t\right) + \frac{V_a-E}{R_a} = 0 + \frac{V_a-E}{R_a}. \tag{55}$$

The equation of the motors in our system is then given by

$$V_a = R_aI_a + E, \tag{56}$$

© 2025 by the author(s). Distributed under a Creative Commons CC BY license.

Preprints.org (www.preprints.org) | NOT PEER-REVIEWED | Posted: 27 February 2026 doi:10.20944/preprints202504.2514.v4

where

$$|E| \equiv k_E \Omega_m. \tag{57}$$

In this equation, the proportionality constant (k_E) depends on the magnetic flux, and (Ω_m) is the rotational velocity.

The current (I_a) is considered as the constant current under zero load (I_{a0}).

Under the working condition:

$$E_{out} > k_B T \tag{58}$$

of our system,

importantly, the motor must satisfy:

$$R_a I_{a0} < k_E \Omega_{m0}, \tag{59}$$

where Ω_{m0} is the speed under zero load.

We now derive the second mandatory condition of the motors. To this end, we discuss the voltages of the motor. At $t = t_c$, because the voltages of the condenser C_0 and voltage source V are canceled, the ohmic input voltage $V_a = 2\varphi_e \equiv 0$ (Eq. (10)). From Eq. (56), we then have:

$$E \equiv E_c = -R_a I_{a0}, \tag{60}$$

meaning that (I_{a0}) is an induced loop current not induced by the voltage source. This equation warrants that the induced current is (I_{a0}). As noted, the above voltage in one motor induces this current in the other motor, implying that the corresponding energy of Eq. (60) in a motor becomes the input to the other motor. Considering this fact and for symmetry, at both the motors, the voltages (E_c) appear.

When the discharge of the induced current is begun by the inductor L, as a generator,

$$E = V_a < 0, \tag{61}$$

where E is the discharging voltage of the inductor L. Notably, as a generator, (V_a) alternatively becomes the output voltage. That is, the input voltage is the voltage (E). However, the voltage of Eq. (61) is common to that of Eq. (60) because the taps providing these voltages are common. This implies that each corresponding electric power is equal.

© 2025 by the author(s). Distributed under a Creative Commons CC BY license.

Preprints.org (www.preprints.org) | NOT PEER-REVIEWED | Posted: 27 February 2026 doi:10.20944/preprints202504.2514.v4

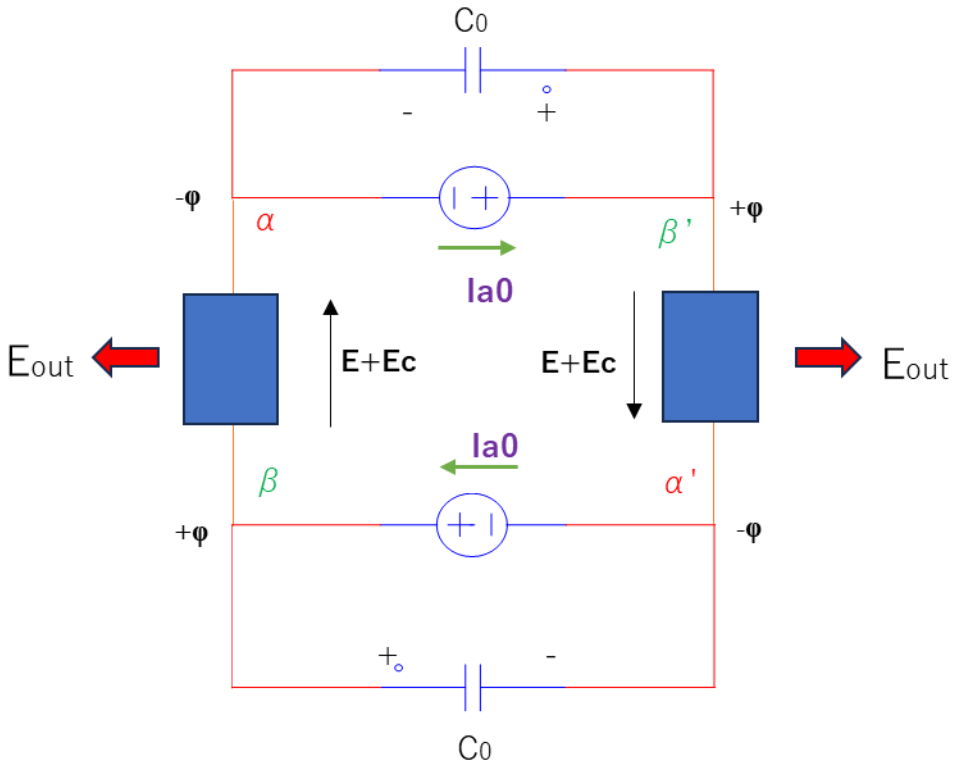

Figure 4. Circuit configuration showing the generation of induced currents (I_{a0}) when the loads are DC motors. As $2\varphi = (E + E_c) > V = 2\varphi_e$ (Results section), the current (I_{a0}) are induced by the inductances of the DC motors. As described for the paired stray capacitors, the paired-inductance L repetitively charge and discharges energy, generating a constant current (I_{a0}) while the voltage sources V steadily decay.

As will be mentioned, the above equation (61) neglects the Joule heating term of Eq. (56). As a result, the motor voltage becomes the superposition of (E_c) and (E), as shown in Figure 4. Thus, the net energy of an electron is (i.e., the updated condenser voltage):

$$E_{out} \equiv e|E + E_c| \equiv 2e\varphi. \qquad (62)$$

To superpose the voltages of Eqs. (60) and (61), the time scale of them must be the same as (t_c), which is not contradictory to the next condition (63).

Let us consider the reason why the Joule heating is neglected. To form the above Eq. (62), i.e., the electric potentials (φ) are emerged, the motors must satisfy:

$$2 \times \frac{1}{2} L I_{a0}^2 > R' i^2 t_c, \qquad (63)$$

where R' denotes the sum of internal resistances of a voltage source and a load. The current (i) of the right side implies the transient ohmic current from the voltage sources; however, it decays when the condition described in Eq. (63) is met. Instead, the current (I_{a0}) appears at $t = t_c$. Considering that Eq. (62) contains the voltage 2φ, implying the voltages for the stray condenser C_0 and inductor L, the condition described in Eq. (63) must be compatible with the condition described in Eq. (3) (Figure 4). That is, the right-sides of both conditions are indirectly equal to that of the voltage source V, and the energies of the stray condenser and inductor must dominate over the energy of the voltage source V. Moreover, because the motors are paired in our system, they reciprocally provide and receive energy. Provided that the second condition above is satisfied, the Joule-heating term is absent and the motor receives a relatively large input voltage near the initial state, as discussed in the Results section. Moreover, we will show that because the voltage of a motor is

$$E_{out}/e \equiv |E + E_c| \equiv 2\varphi > V = 2\varphi_e, \qquad (64)$$

implying that the voltage sources V are nonoperational, the loop current (I_{a0}) is conserved steadily.

© 2025 by the author(s). Distributed under a Creative Commons CC BY license.

Preprints.org (www.preprints.org) | NOT PEER-REVIEWED | Posted: 27 February 2026 doi:10.20944/preprints202504.2514.v4

The macroscopic current (I_{a0}) can coexist with the microscopic current (I'_E) in the load but the two currents are not superposed, so an additive current does not appear. Thus, if a current meter is connected in series with a motor, it records either the current (I_{a0}) or the current (I'_E) at each moment, presenting widely fluctuating currents to the experimental observer. Accordingly, we set a detour for the current (I'_E) in the system with paired DC motors (Figure 5). In the Results section, we will discuss the importance of:

$$I'_E \gg I_{a0}. \tag{65}$$

Here, let us introduce the output electric power (W_{R0}). The incremental value in the right-side motor in Figure 5 is

$$dW' \equiv I'_E(0) \times 2d\varphi, \tag{66}$$

where

$$I'_E(0) \equiv 0.45\left(\frac{E+E_c}{2}\right)^2 = const.. \tag{67}$$

Considering the symmetry in Figure 5, i.e., because the voltage $(2d\varphi)$ in the right-side motor is essentially equal to that of the left-side motor, Eq. (66) must equal to the incremental electric power (dW) in the left-side motor.

Generally, we have, in the resistance and in the left motor of Figure 5,

$$2d\varphi_{\alpha,\beta} = R_0 dI'_E \text{ and } d\varphi_{\alpha,\beta} \equiv pd\varphi. \tag{68}$$

That is,

$$2d\varphi = \frac{R_0}{p} dI'_E, \tag{68-2}$$

where p is the proportional constant. The reason to introduce this constant will be discussed in the Discussion section. Eqs. (68) and (68-2) imply the current (I'_E) is common to the left motor and the resistance. Considering Eq. (66),

$$dW = I'_E(0)\frac{R_0}{p} dI'_E. \tag{69}$$

Given $I'_E = 0.45\varphi^2$ of the left-side motor, we obtain

$$dW = I'_E(0)\frac{R_0}{p} \times d(0.45\varphi^2) = 0.45I'_E(0)\frac{R_0}{p} \times 2\varphi d\varphi. \tag{70}$$

Integrating both sides of Eq. (70) gives

$$W_{R0} = 0.45R_0 I'_E(0)\varphi^2 \text{ [W]}, \tag{71}$$

where W_{R0} is the electric power in the resistance (R_0) defined by $W_{R0} = pW$.

Given that the conditions in our system are satisfied, Eq. (71) is not a Joule-heating expression.

The absence of Joule heating can be explained by dead voltage sources, as is frequently described herein. The voltage sources are only temporarily active in the period close to the initial time (Figure 1).

Although a general current (I'_E) was considered, and because this current is common to the resistance and the left motor—which is, for symmetry, equal to that of the right-side motor $I'_E(0)$—the derivation that results in Eq. (71) indicates that $I'_E(0)$ in the left-side motor follows the path of the resistance (R_0) instead of the path of the left-side motor. Note that (I'_E) cannnot coexist simultaneously in the left motor and resistance because of Kirchhoff's current law. Alternatively, the current $I'_E(0)$ in the right-side motor is continuous to the current along the load (R_0), through the stray condensers C_0.

© 2025 by the author(s). Distributed under a Creative Commons CC BY license.

Preprints.org (www.preprints.org) | NOT PEER-REVIEWED | Posted: 27 February 2026 doi:10.20944/preprints202504.2514.v4

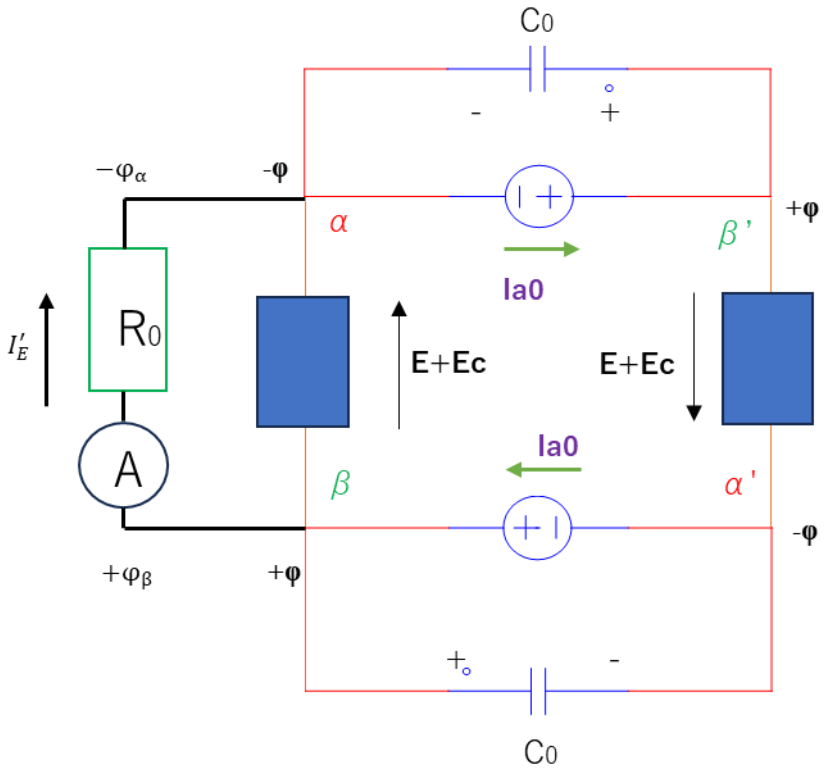

Figure 5. Harvesting of the divergent current (I'_E) in the system with DC motor loads. The macroscopic current (I_{a0}) interferes with the microscopic current (I'_E), necessitating a detour. As described in the main body, it can be interpreted that the current $I'_E(0)$ in the left-side motor alternatively chooses the detour: The emergent electric potential $|\varphi| = \left|\frac{E+E_c}{2}\right| = const.$ provides a constant current $I'_E = 0.45(\frac{E+E_c}{2})^2, which$ is independent of the resistance (R_0). Therefore, a large resistance (for example, 1.0 MΩ) allows the current flow. For the same reason, this equation is not an ohmic equation so Joule heating is absent. Note that $|\varphi_{\alpha,\beta}|$ will be described in the Discussion section.

3. Results

We first present the results of the paired-LED system with:

$E_{out} \equiv 2e\varphi$ (72)

or

$E_{out} \equiv \hbar\omega,$ (73)

where ω is the angular frequency. The divergent current is

$I'_E = 0.04(\frac{\hbar\omega}{2e})^2.$ (74)

Given the approximate wavelength (λ) of a blue LED:

$\lambda = 460$ [nm], (75)

the angular frequency is calculated as

$\omega = \frac{2\pi c}{\lambda} \approx 4.1 \times 10^{15}$ [rad/s]. (76)

Thus,

$I'_E = 0.04\varphi^2 = 0.04(\frac{\hbar\omega}{2e})^2 \approx 0.04 \times (1.34)^2 \approx 71$ [mA]. (78)

The voltage is

$2 \times 1.34 = 2.68$ [V]. (79)

The above current and voltage are valid.

The results of the LED system are summarized in the following three figures (Figures 6-1–6-3): a schematic configuration of the circuit, a photograph of the initial experimental setup, and a photograph of the experimental result.

© 2025 by the author(s). Distributed under a Creative Commons CC BY license.

Preprints.org (www.preprints.org) | NOT PEER-REVIEWED | Posted: 27 February 2026 doi:10.20944/preprints202504.2514.v4

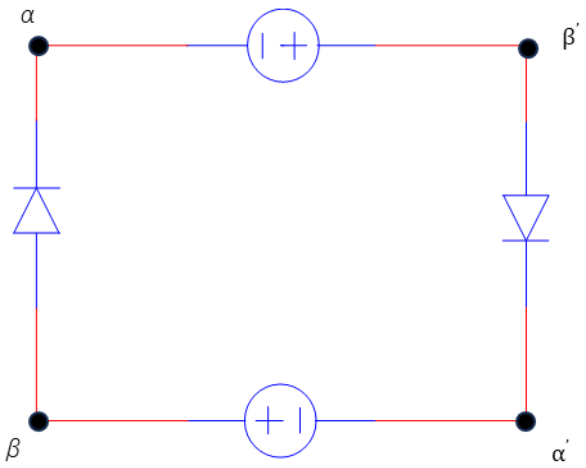

Figure 6-1. Schematic of divergent current (I'_E) generation in the system with LED loads. As described in the main text, the divergent current (I'_E) drives the LEDs and the voltage sources die at steady-state.

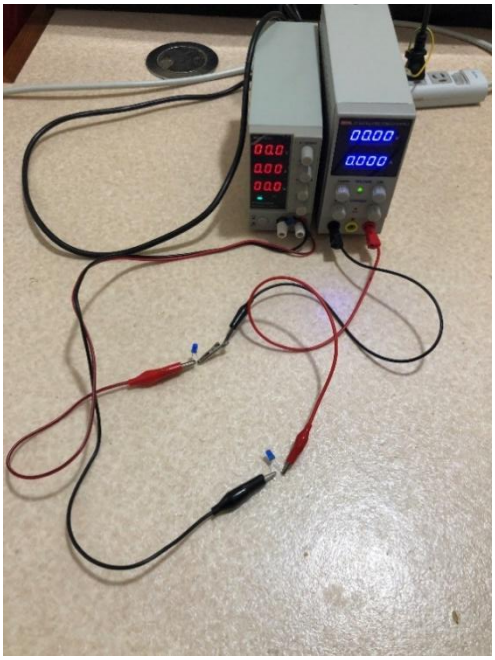

Figure 6-2. Initial setting of the experiment for confirming operation of the LED pair. The setup includes two power supplies (voltage sources) and two blue LEDs.

© 2025 by the author(s). Distributed under a Creative Commons CC BY license.

Preprints.org (www.preprints.org) | NOT PEER-REVIEWED | Posted: 27 February 2026 doi:10.20944/preprints202504.2514.v4

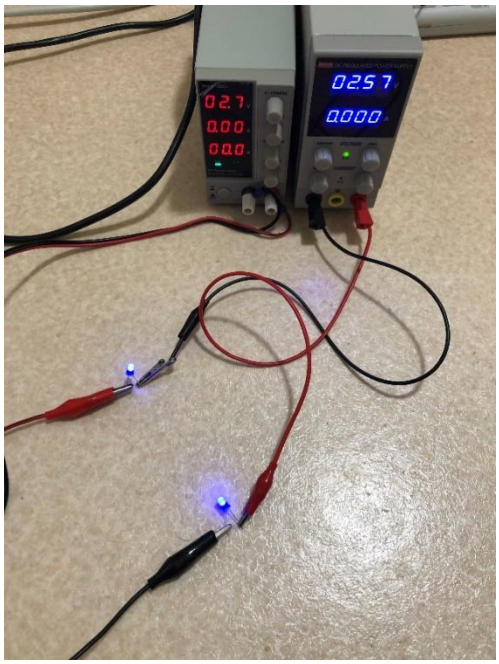

Figure 6-3. Experimental result of the system with two LED loads. The paired-LED is working and the current in the voltage sources is almost zero, confirming the appearance of the divergent current (I'_E) and decay of the net voltage sources.

We now present the results of the paired motor system.

Table 1 lists the specifications of the employed DC motor, and Figures 7 and 8 show a potable tester and the employed paired motors, respectively.

Table 1. Motor specifications of the MABUCHI motor (RE-280RA).

Normal voltage	3.0 V
Normal Load	1.47 mN · m
Speed at no Load	8,700 r/min
Speed at normal Load	5,800 r/min
Current at normal load	650 mA
Shaft Diameter	2.0 mm

© 2025 by the author(s). Distributed under a Creative Commons CC BY license.

Preprints.org (www.preprints.org) | NOT PEER-REVIEWED | Posted: 27 February 2026 doi:10.20944/preprints202504.2514.v4

Figure 7. Photograph of our tester, included for the reasons given in the Discussion.

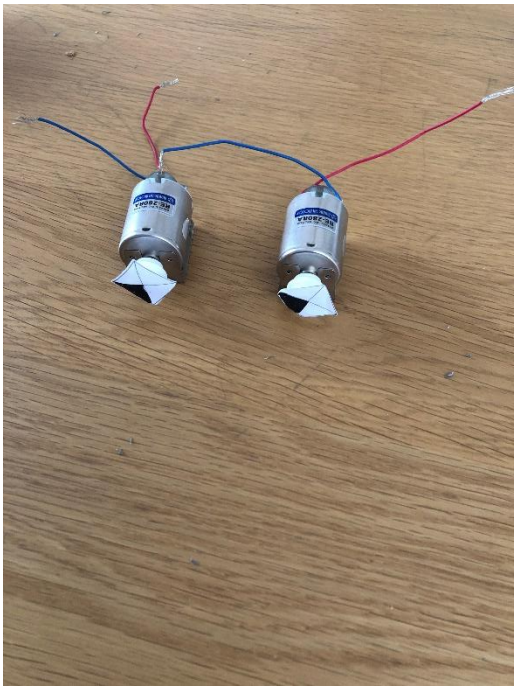

Figure 8. Photograph of the paired DC motors (MABUCHI motor RE-280RA), marked with black dots to confirm whether the motors rotate during the experiment.

Figures 9 and 10 present the three stages of the paired motor experiments: the circuit configurations, the preparations of the experiments, and the experimental results.

© 2025 by the author(s). Distributed under a Creative Commons CC BY license.

Preprints.org (www.preprints.org) | NOT PEER-REVIEWED | Posted: 27 February 2026 doi:10.20944/preprints202504.2514.v4

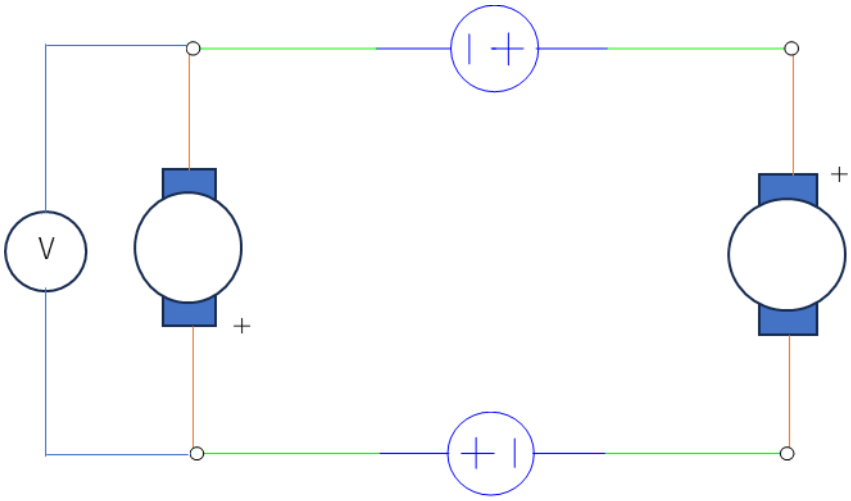

Figure 9. Schematic of the circuit for measuring an emergent electric potential. The voltage of the voltage source is compared with that of the DC motor, which implies the emergent electric potential (φ).

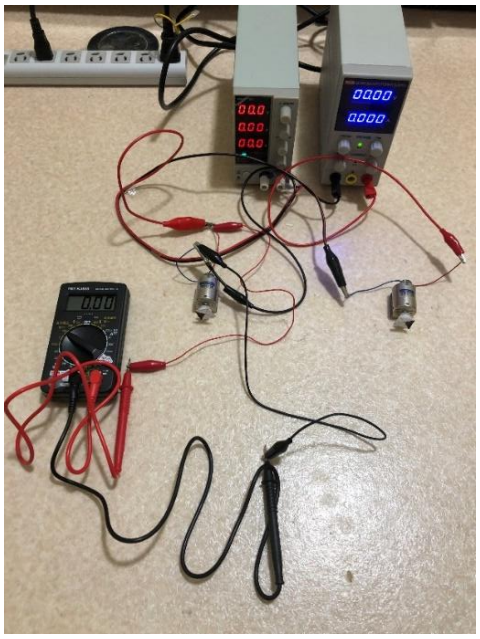

Figure 9-2. Experimental setup for measuring the emergent electric potential (φ). The voltage sources are two stabilized power supplies, one with a red light display; the other with a blue display. The two DC motors are not rotating at this time, as evidenced by the stationary black dots. The emergent electric potential is measured by a voltmeter (foreground).

© 2025 by the author(s). Distributed under a Creative Commons CC BY license.

Preprints.org (www.preprints.org) | NOT PEER-REVIEWED | Posted: 27 February 2026 doi:10.20944/preprints202504.2514.v4

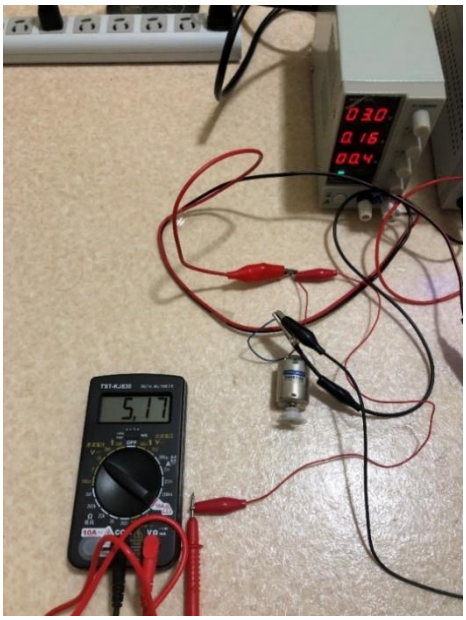

Figure 9-3. A result of the experimental setup in Figure 9-2. When the voltage source displays 3.0 V, the voltage associated with the emergent electric potential is 5.17 V, approximately 40% larger than the source voltage. From this result, it is evident that the current (I_{a0}) is induced current not ohmic one.

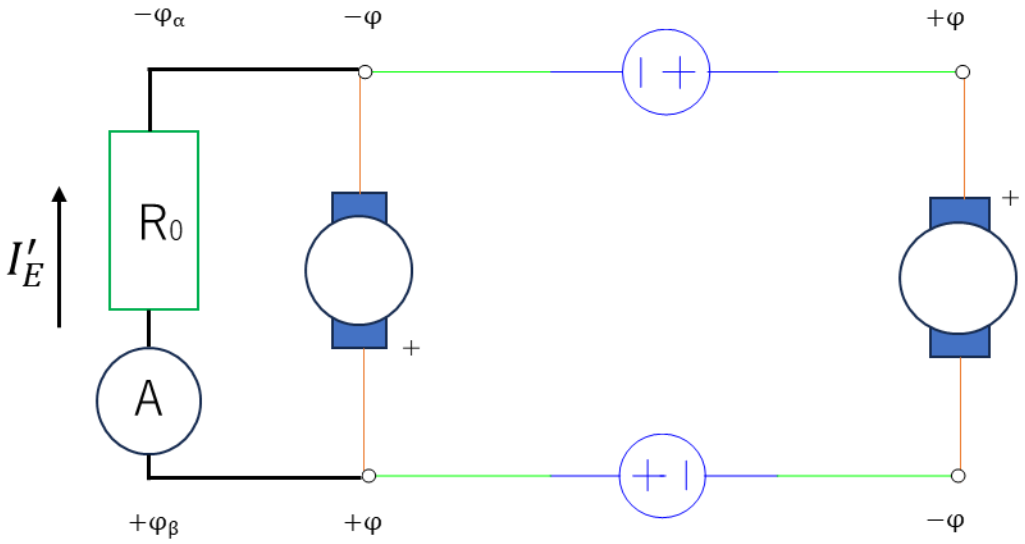

Figure 10-1. Circuit configuration of the experiment for harvesting the current (I'_E). As in Figure 5, a detour avoids interference between the induced macroscopic current (I_{a0}) and the microscopic current (I'_E). As the mathematical form of the current $I'_E(0)$ is independent of the load (R_0) and differs from Ohm's law, the current flows even when the load (R_0) is large. For the same reason, the load resistance (R_0) generates no Joule heating. Note that $|\varphi_{\alpha,\beta}|$ will be described in the Discussion section.

© 2025 by the author(s). Distributed under a Creative Commons CC BY license.

Preprints.org (www.preprints.org) | NOT PEER-REVIEWED | Posted: 27 February 2026 doi:10.20944/preprints202504.2514.v4

Figure 10-2. Initial setup of the experiment for harvesting the current (I'_E). Shown are the two voltage sources, the paired motors, a current meter (range 10 A), and a 1.0-MΩ resistor connected by the red and yellow leads (in the vicinity of the left motor).

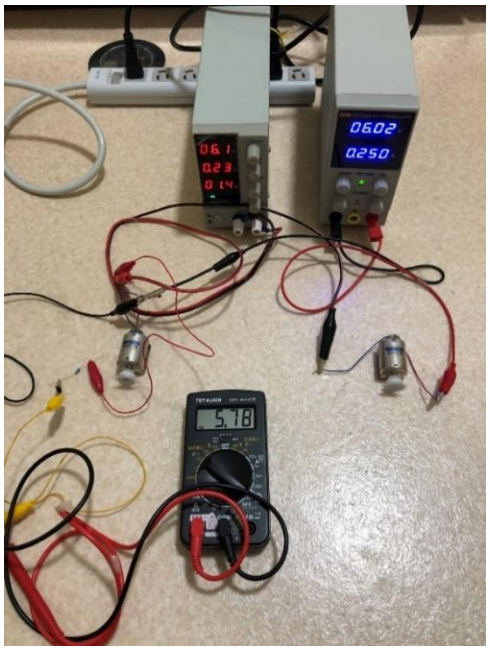

Figure 10-3. Experimental result when the initial input voltage is ~6.0 V. The divergent current (I'_E = 5.78 A) is much larger than the induced current (I_{a0} ≈ 0.24A).

© 2025 by the author(s). Distributed under a Creative Commons CC BY license.

Preprints.org (www.preprints.org) | NOT PEER-REVIEWED | Posted: 27 February 2026 doi:10.20944/preprints202504.2514.v4

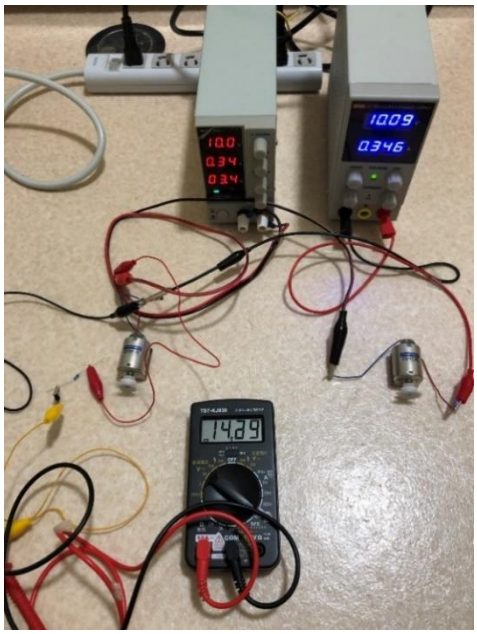

Figure 10-4. Experimental result when the initial input voltage is 10.0 V. The current meter reads I'_E >14 A, much larger than the induced current I_{a0}(≈ 0.34 A). Even when the load is very large (1.0 MΩ), a substantially large current is flowing. Note that no Joule heating occurs in the motors, and a relatively large input voltage is allowed. That is, these motors can be repeatedly used even when the input voltage exceeds 3.0 V.

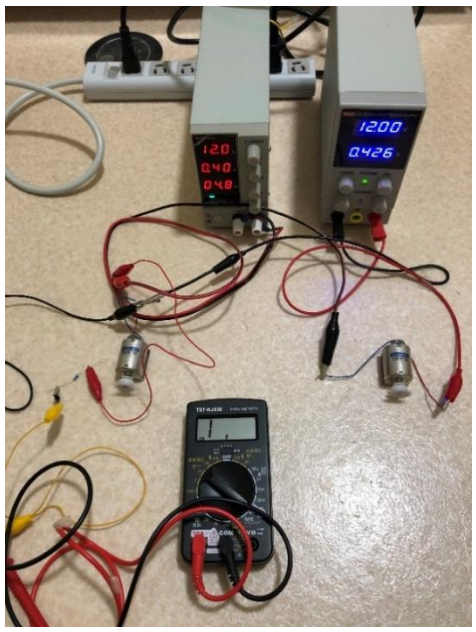

Figure 10-5. Experimental result when the initial input voltage is 12.0 V. The divergent current (I'_E) is out-of-range, implying that it exceeds 20.0 A through the 1.0-MΩ load.

© 2025 by the author(s). Distributed under a Creative Commons CC BY license.

Preprints.org (www.preprints.org) | NOT PEER-REVIEWED | Posted: 27 February 2026 doi:10.20944/preprints202504.2514.v4

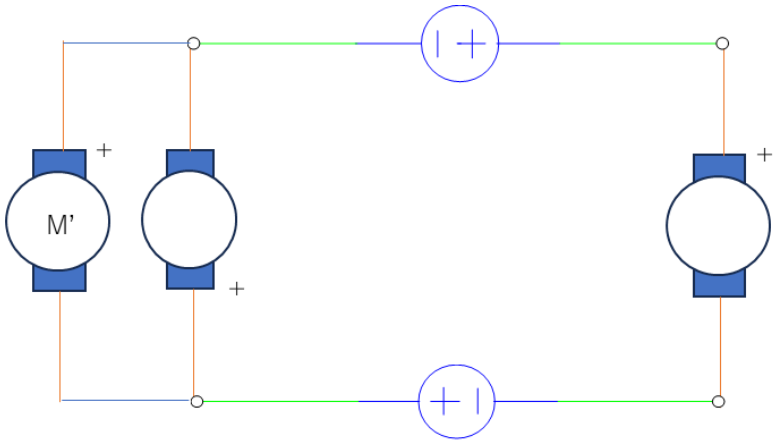

Figure 11. Circuit configuration after inserting another motor as a detour. Note that the polarity (i.e. the direction) of each motor is important. That is, the polarity of M′ must be reversed from that of the paired motors and motor M′ rotates oppositely to the paired motors. If configured otherwise, M′ will not rotate. The photograph is omitted because motor M′ is not easily distinguishable; therefore, the photograph is noninformative.

Table 2 compares the experimentally observed currents $I'_E(0)$ with the theoretical currents determined as

$$I'_E(0) \equiv 0.45\left(\frac{E+E_c}{2}\right)^2, \quad (80)$$

where $(E + E_c)/2$ is the emergent electric potential (φ) with

$$\varphi > \varphi_e = V/2. \quad (81)$$

As the emergent electric potential must not be significantly larger than of the input electric potential (φ_e), we approximate

$$\left|\frac{E+E_c}{2}\right| \approx 1.2\varphi_e \quad (82)$$

as a compromise. As shown, Table 2 confirms sufficient agreements between the experimental and theoretical values.

Table 3 lists the generated electric power (W_{R0}) for different input voltages ($2\varphi_e$). The electric potential (φ) in Eq. (71) is defined again by Eq. (82). The values of the electric powers in Table 3 are sufficiently large and are almost equivalent to those of nuclear power stations, implying that the values presented in Table 3 have significant technical merit.

For confirmation, we validate Eq. (71); that is,

$$W_{R0} = 0.45R_0I'_E(0)\varphi^2, \quad (83)$$

in the paired motor system. The electric power of the LED is obtained simply by replacing coefficient 0.45 [A/V²] with 0.04 [A/V²] as

$$W_{LED} = 0.04R_0I'_E(0)\varphi^2. \quad (84)$$

Assuming

$$I'_E(0) = 71\ [\text{mA}] \quad (85)$$

and

$$\varphi = 1.34\ [\text{V}], \quad (86)$$

we obtain

$$R_0 = \frac{2\times 1.34V}{71mA} \approx 38\ [\Omega], \quad (87)$$

from which W_{LED} is calculated as

$$W_{LED} \approx 0.193\ [\text{W}]. \quad (88)$$

Meanwhile, the direct electric power W'_{LED} is defined as simply

$$W'_{LED} \equiv I'_E \times 2\varphi. \quad (89)$$

Then we get:

$$W'_{LED} \approx 0.190\ [\text{W}]. \quad (90)$$

© 2025 by the author(s). Distributed under a Creative Commons CC BY license.

Preprints.org (www.preprints.org) | NOT PEER-REVIEWED | Posted: 27 February 2026 doi:10.20944/preprints202504.2514.v4

Thus

$$W_{LED} \approx W'_{LED}, \quad (91)$$

validating the expression of W_{LED}. Considering that Eq. (83) (i.e., Eq. (71)) differs only in the coefficient (i.e., $0.04 \rightarrow 0.45$), it is allowed to mention that the above result (91) also validates Eq. (71).

Table 2. Comparisons of the experimental and theoretical currents $I'_E(0)$ based on the previous results.

$2\varphi_e$[V]	$I'_E[A]$ for the theory	$I'_E[A]$ for the experiment
6.0	5.8	5.78
10.0	16.2	14.3
12.0	23	More than 20

Table 3. Output electric power (W_{R0}) evaluated for a 1.0-MΩ load resistance (R_0) and the theoretical divergent currents $I'_E(0)$ listed in Table 2.

$2\varphi_e$[V]	W_{R0} [W]
6.0	3.3×10^7
10.0	2.6×10^8
12.0	5.4×10^8

Figure 11 shows the circuit configuration when another motor is employed as the detour. The detour motor operated only when its polarity was reversed from that of the paired motors. In this configuration, the additional motor exchanged energy with the paired stray condensers. The exchanged energy is

$$U_M = \frac{1}{2} L I'^2_E, \quad (92)$$

For confirmation, the details of the experimental instruments are specified in Table 4

Table 4. Specifications of experimental instruments.

Instruments	Manufacturer	Model	Country
Digital multimeter	Ohm-Denki	TST-KJ830	Japan
DC power supply 1	WANPTEK	NPS306W	Japan
DC power supply 2	MCH	MCH-K3010DN	Japan
DC motor	MABUCHI	RE-280RA	Japan

4. Discussion

4.1. Why can a large current flow into the 1.0-MΩ resistor?

A circuit containing a resistance (R) typically exhibits ohmic characteristics, meaning that its current depends on (R). However, in the present study,

$$I'_E(0) \equiv 0.45 \left(\frac{E+E_c}{2}\right)^2 = const., \quad (80)$$

which is independent of the resistance (R), meaning that the current flows through any resistor. The large current flow through the 1.0-MΩ resistor is explained not only by this phenomenon, but also by the absence of Joule heating under the imposed conditional inequalities.

© 2025 by the author(s). Distributed under a Creative Commons CC BY license.

Preprints.org (www.preprints.org) | NOT PEER-REVIEWED | Posted: 27 February 2026 doi:10.20944/preprints202504.2514.v4

4.2. Condition and selection of the paired motor

To ensure that the paired DC motors satisfy the conditional inequalities (59) and (63), we recommend motors with relatively large inductances. However, inductors with excessive inductance should be avoided because they increase the internal resistance. Therefore, the paired DC motors must be carefully selected. This paper employs the previously discussed MABUCHI motor RE-280RA. A trial experiment using coreless motors as the paired DC motors failed to display the phenomenon described here, possibly because coreless motors with relatively small inductances cannot satisfy the requisite conditions (59) or (63).

4.3. Why is a relatively large resistance needed when harvesting the current?

To answer this question, we revisit Eq. (80):

$I'_E(0) \equiv 0.45\left(\frac{E+E_c}{2}\right)^2$,

which implies that the voltage between taps α and β is $(E + E_c)$ [V]. When harvesting the current through a detour, the resistance (R_0) should be sufficiently large to satisfy (Figure 10-1)

$$\left|\varphi_{\alpha,\beta}\right| \geq \left|\frac{E+E_c}{2}\right|, \quad (93)$$

where the left side is the electric potential at tap α or β owing to the flow of the current $I'_E(0)$ to the resistance (R_0). Even when the condition described in Eq. (93) is met, the emergent electric potential $|\varphi|$ at each tap remains $\left|\frac{E+E_c}{2}\right|$ because the current $I'_E(0)$ must be constant and not increase. This is because, considering that Eq. (57) is formed and that no Joule heating implies motor load of zero, the zero-load motor implies that the rotational speed (Ω_m) is at the maximum value (Ω_{m0}). Thus, the absolute value of the voltage (E) under a zero load is the maximum value. Therefore, the voltage of the motor, $|E + E_c|$, is conserved. Thus, the electric potentials $\left|\varphi_{\alpha,\beta}\right|$ are not superposed at each tap. Assume another stray condenser C_{0R} parallel to both sides of the paired motors: the stray condenser C_{0R} of the left side retains the electric potentials $\left|\varphi_{\alpha,\beta}\right|$ by charging energy; Although the resultant $\left|\varphi_{\alpha,\beta}\right|$ appears, the electric potentials $|\varphi|$do not increase as described. That is, they are not superposed.

If the condition described in Eq. (93) is satisfied, the current $I'_E(0)$ takes the path along the detour instead of the motor path. This can be proved by the fact that initially the motor inductor L generates magnetic field energy from the current $I'_E(0)$; thus, to reduce this energy to zero in the inductance, the current $I'_E(0)$ chooses the resistance (R_0) path. Notably, if this condition is not satisfied, and because a current is discharged from the inductor L of the left motor to the resistance (R_0) owing to a decrease in the absolute value of the voltage (E), the current $I'_E(0)$ forms a loop current along R_0-L and decreases to almost zero. To meet the condition described in Eq. (93), a relatively large resistance must be used as the detour.

When a current meter is placed along the detour, the electric potential at both the taps α and β should also satisfy the above condition. According to Figure 10-1, a relatively large load (R_0) will enlarge the electric potential (φ_α). Moreover, our tester with a relatively large flow divider of a 10-A range is justified for boosting the electric potential (φ_β). Note that, if a current meter that is to detect a small current is employed, the electric potential (φ_β) becomes small.

Moreover, the phenomenon detected in the many experiments of this paper could not be detected by an auto range detector. Such a detector should be employed in a follow-up study, but an internal resistance that varies with the electrical signals might violate the above condition (93). Perhaps, there is a macroscopic current (i_A) in auto range meter and thus this current (i_A) might interfere with the microscopic current (I'_E). Therefore, an auto range meter was not employed in our present experiments (Figure 7).

When another motor M' is employed as a detour, energy exchanges between the inductor and the stray condensers give rise to a constant current (I'_E). As the additional motor has a very small internal resistance, it demonstrates the potential of supplying the current (I'_E) to a small resistance via the observed phenomenon.

© 2025 by the author(s). Distributed under a Creative Commons CC BY license.

Preprints.org (www.preprints.org) | NOT PEER-REVIEWED | Posted: 27 February 2026 doi:10.20944/preprints202504.2514.v4

4.4. Discussion of the generation of energy

Let us consider the process of harvesting the electric power in terms of physics. First, for the input electric potential (φ_e), the minimum uncertainty relation is expressed as follows:

$(e\varphi_e) \times t = \frac{1}{2}\hbar.$ (94)

That is,

$t = \frac{\hbar}{2e\varphi_e},$ (94-2)

where t denotes the transition time. In this section, for example, the input electric potential (φ_e) is assumed to be 5.0 V consistently.

Let us consider the process of generating energy more concretely.

According to Figure 2, the position between the taps α and β' implies the vacuum (i.e., a stray condenser). Thus, the energy gap of the vacuum from the Dirac equation is required to be considered:

$\hbar\omega = 2mc^2,$ (95)

where ω, m, and c denote the angular frequency, the mass of an electron or a positron and the speed of light, respectively.

This equation is interpreted as

$\frac{1}{2}\hbar\omega = mc^2.$ (96)

As every basic quantum theory textbook defines, the left side of this equation is the zero-point energy, which is a part of the Hamiltonian of a harmonic oscillator.

From Eq. (94),

$(e\varphi_e)t = \frac{mc^2}{\omega}.$ (97)

$\omega \equiv \frac{\theta}{t}.$ (98)

Thus,

$\theta = \frac{mc^2}{e\varphi_e},$ (99)

Note that (φ_e) is defined as 5.0 V in this section, for example.

As shown in the above equation, this parameter (θ) works as the interchanges between a circuit energy and the vacuum energy (Figure 12). In Figure 12, owing to the existence the current (i), we assume that the energy flows from tap α to tap β'. Note that the dual figure for Figure 12 exists between taps α' and β. Thus, according to Figure 12, because the energy flows from tap α to tap β',

$\theta = \frac{P'_{out} \times t}{mc^2}.$ (100)

Form Eq. (94-2),

$t = \frac{\hbar}{2e\varphi_e} \approx 6.5 \times 10^{-17}[\mathrm{s}].$ (101)

Thus,

$P'_{out} \approx 1.2 \times 10^{8}[\mathrm{W}].$ (102)

The above electric power implies, at an extremely short time, the energy increases as follows:

$P'_{out} \equiv \varphi'' \times I''_E.$ (103)

The reason for the increase will be described later.

Considering the dural figure for Figure 12, the net electric power is

$P_{out} \equiv 2P'_{out} \approx 2.4 \times 10^{8}[W] \rightarrow W_{R0},$ (104)

where the created electric power is transformed the load's electric power (W_{R0}) in Eq. (71). This value is consistent with the value of Table 3 (for $2\varphi_e \equiv 10.0\,V$). This implies that the temporally increased electric power Eq. (103) transformed to the load power Eq. (71).

Let us consider the reason the electric potential (φ'') and the current (I''_E) in Eq. (103) decrease to (φ) and (I'_E) in (W_{R0}) in Eq. (71) at the steady state.

i) At the transient state near the initial time, the impedance (Z_c) of a stray condenser is almost shorted and thus the current increases temporally to (I''_E). However, at the steady state, because the value of the impedance (Z_c) is restored to the normal value, implying that the current decreases to (I'_E).

© 2025 by the author(s). Distributed under a Creative Commons CC BY license.

Preprints.org (www.preprints.org) | NOT PEER-REVIEWED | Posted: 27 February 2026 doi:10.20944/preprints202504.2514.v4

ii) In Eqs. (103) and (104),

$$2P'_{out} = (2\varphi'') \times I''_E \equiv V_R \times I''_E \ , \qquad (105)$$

where the voltage V_R denotes one in the load, which essentially equal to the electric potential $|\varphi_{\alpha,\beta}|$. Because the electric potentials $|\varphi|$ are dependent on $|\varphi_{\alpha,\beta}|$, the electric potentials $|\varphi|$ also appear (Eq. (68)).

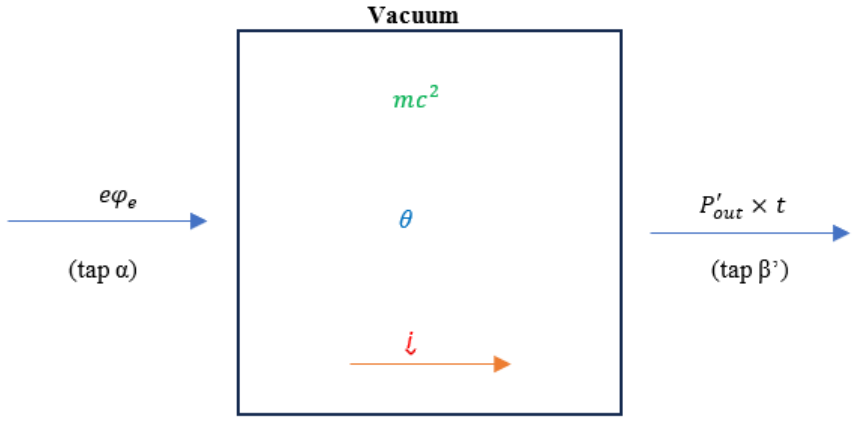

Figure 12. Transient vacuum model in our system. This figure indirectly expresses a stray condenser between taps α and β'. Note that there is the dual figure between taps α' and β. The energy $(e\varphi_e)$ implies the input energy and (P'_{out}) denotes the temporal output electric power, and (t) is the time. Moreover, (mc^2) indirectly implies the energy of the vacuum. The parameter (θ) is the converting parameter between an electric circuit energy and the vacuum energy. Furthermore, the current (i) is the transient state current.

Considering the above discussion, the transient time (t) is essentially equal to the transition time (t_c) in this paper.

Let us consider the reason for generating this energy.

In quantum mechanics, the following general uncertainty relation holds:

$$\Delta E \Delta t \geq \frac{1}{2}\hbar, \qquad (106)$$

where E and t denote the energy and the time, respectively.

Alternatively,

$$\Delta E \geq \frac{1}{2}\hbar \frac{1}{\Delta t}. \qquad (106\text{-}2)$$

This equation implies that, only during the time (Δt), it is allowed to consider that the energy is not conserved. Importantly, this fact is only in quantum mechanics, not in classical mechanics.

In this equation, the minimum equation corresponds to Eq. (94). That is,

$$\Delta t \equiv \frac{\hbar}{2e\varphi_e}. \qquad (107)$$

When (Δt) is considered to be common, for the excited energy (ΔE) and to form the inequality,

$$\Delta E \neq e\varphi_e. \qquad (108)$$

Thus, approximately,

$$\Delta E \approx U'_{out}, \qquad (109)$$

where U'_{out} denotes the output energy.

Thus,

$$U'_{out} \times \frac{\frac{1}{2}\hbar}{e\varphi_e} > \frac{1}{2}\hbar. \qquad (110)$$

That is,

$$U'_{out} > e\varphi_e. \qquad (111)$$

This equation concludes that the output energy of the system is larger than the input energy. As mentioned, this relation (i.e., the uncertainty relation) is the unique property only in quantum mechanics. The classical mechanics lacks this property. The mass of a π-meson was calculated under the same nonenergy conservation by H. Yukawa.

© 2025 by the author(s). Distributed under a Creative Commons CC BY license.

Preprints.org (www.preprints.org) | NOT PEER-REVIEWED | Posted: 27 February 2026 doi:10.20944/preprints202504.2514.v4

4.5. Symmetric circuit operation

Let us consider a method for controlling the symmetric circuit. For example, let us consider the case where the two voltage sources are set to 8.0 [V]. First, a voltage source is set to 8.0 V. Then, the other voltage source volume is increased gradually. During this process, the output current (I'_E) is almost zero in the current meter at first; however, when the volume reaches around 7.0 V, the output current suddenly appears. In view of several experiences, the difference of the outputs of the two voltage sources is allowed to be within $0.1 - 0.5$ V. However, the reason for this allowance should be follow-up.

4.6. Recap of the key concept

This paper describes a novel concept and a highly symmetric circuit for renewable energy generation. A circuit satisfying the requisite conditions generates a divergent current with no Joule heating. The divergent current drives both paired-LED and paired-DC-motor systems, generating large amounts of energy. The phenomenon is demonstrated both theoretically and experimentally, with good agreement between the theoretical and experimental results.

4.7. Significances of this paper

Many countries are attempting to mitigate the pending energy crisis with solar cells, wind power, and biomass energy sources. However, natural energy produced by renewable energy sources inevitably fluctuate and destabilize the energy system. Stability can be restored only by introducing many storage batteries that increase the costs. More seriously, fossil fuel energies are major CO_2 emitters, whereas nuclear power stations (which release no CO_2) destroy the environment with radioactive materials and their wastes.

Our proposed methodology generates a large amount of energy using a highly symmetric circuit. The main contributions are listed below.

1) The net generated energy almost equals that of a nuclear power station, implying a sufficiently high energy density.
2) The system can be introduced at low-cost (<10,000 yen).
3) The system generates no dangerous substances.
4) The experiments in this paper do not require a large area of space for infrastructure. For example, besides the standard receptacles, a standard experimental table to place the two voltage sources $(1.5\ m \times 1.5\ m)$ is only required.
5) This system can provide the required amount of energy at the right time at the right place.

In summary, our simple-to-build system generates comparable energy to a nuclear power station.

5. Conclusions

This study proposes and verifies (theoretically and experimentally) a new circuit-based renewable energy source. The system outputs a very high electric power and high energy density without natural fluctuations or dangerous substance production. That is, it harvests the required amount of energy at the proper time at the proper place.

Various motor types were experimentally trialed in the paired motor system, but a more systematic experiment would consolidate the aforementioned conditions. Moreover, the capacitance of the stray capacitor is expected to slightly vary with humidity and atmospheric pressure. This expectation must be clarified in future work. Importantly, physical mechanisms for generating the macroscopic current (I_{a0}) in the DC motor pair, which has no Joule heating, will be required to be identified. Finally, the inapplicability of the auto range meter must be rationalized.

© 2025 by the author(s). Distributed under a Creative Commons CC BY license.

Preprints.org (www.preprints.org) | NOT PEER-REVIEWED | Posted: 27 February 2026 doi:10.20944/preprints202504.2514.v4

Funding: This research received no external funding.

Data Availability Statement: All original contributions and data associated with this study are included in the article. All data (raw) are presented as photographs in the Results section. Further inquiries can be directed to the corresponding author

Acknowledgments: We thank Enago (www.enago.jp) for the English language reviews. In addition, we appreciate the release of the preprints of the first, second and third versions.: Ishiguri, S. Experimental Evidence of High Renewable Energy Employing a Symmetric Circuit with a Divergent Current Density. Preprints 2025, 2025042514. https://doi.org/10.20944/preprints202504.2514.v1 https://doi.org/10.20944/preprints202504.2514.v2; https://www.preprints.org/manuscript/202504.2514/v3

Conflicts of Interest: The authors declare no conflicts of interest.

Abbreviations

The following abbreviations are used in this manuscript:

LED	Light-emitting diode
DC	Direct current

References

1. Osman, A.I.; Chen, L.; Yang, M.; Msigwa, G.; Farghali, M.; Fawzy, S.; Rooney, D.W.; Yap, P.S. Cost, environmental impact, and resilience of renewable energy under a changing climate: a review. *Environ. Chem. Lett.* **2023**, *21*, 741–764. Doi: 10.1007/s10311-022-01532-8.
2. Suresh Lal, S.R; Joselin Herbert, G.M.; Arjunan, P.; Suryan, A. Advancements in renewable energy transition in India: a review. *ESAO* **2025**, *47*, 2024921. Doi.10.1080/15567036.2021.2024921
3. Nassar, Y.F.; El-khozondar, H.J.; Ahmed, A.A.; Alsharif, A.; Khaleel, M.M.; El-Khozondar, R.J. A new design for a built-in hybrid energy system, parabolic dish solar concentrator and bioenergy (PDSC/BG): a case study–Libya. *J. Clean. Prod*. **2024**, *441*, 140944. Doi: 10.1016/j.jclepro.2024.140944.
4. Guo, A.; Dai, J.; Chang, J.; Wang, Y.; Deng, X.; Wang, X. Coordinated peak shaving of open-loop pumped-storage and conventional hydropower plants: multiple operation modes, optimal operating boundaries and associated impacts. *Energy Conv. Manag*. **2025,** *345*, 120386. Doi: 10.1016/j.enconman.2025.120386.
5. Sadiq, M.; Hassan, S.T.; Khan, I.; Rahman, M.M. Policy uncertainty, renewable energy, corruption and CO_2 emissions nexus in BRICS-1 countries: a panel CS-ARDL approach. *Environ. Dev. Sustain*. **2024**, *26*, 21595–2162. Doi: 10.1007/s10668-023-03546-w.
6. Abdulqadir, I.A. Urbanization, renewable energy, and carbon dioxide emissions: a pathway to achieving sustainable development goals (SDGs) in sub-Saharan Africa. *Int. J. Energy Sect. Manag*. **2024**, *18*, 248–270. Doi: 10.1108/IJESM-11-2022-0032.
7. Obane, H.; Nagai, Y.; Asano, K. Assessing land use and potential conflict in solar and onshore wind energy in Japan. *Renew. Energy*. **2021**, *160*, 842–851. Doi:10.1016/j.renene.2020.06.018
8. Zahedi, R.; Sadeghitabar, E.; Khazaee, M.; Faryadras, R.; Ahmadi, A. Potentiometry of wind, solar and geothermal energy resources and their future perspectives in Iran. *Environ. Dev. Sustain*. **2025**, *27*, 15311–15337. Doi: 10.1007/s10668-024-04633-2.
9. Sabishchenko, O.; Rębilas, R.; Sczygiol, N.; Urbański, M. Ukraine energy sector management using hybrid renewable energy systems. *Energies* **2020**, *13*, 1776. doi:10.3390/en13071776.
10. Adebayo, T.S.; Oladipupo, S.D.; Adeshola, I.; Rjoub, H. Wavelet analysis of impact of renewable energy consumption and technological innovation on CO_2 emissions: evidence from Portugal. *Environ Sci Pollut Res*. **2022**, *29*, 23887–23904. Doi: 10.1007/s11356-021-17708-8.
11. Wang, C.-N.; Tibo, H.; Duong, D.H. Renewable energy utilization analysis of highly and newly industrialized countries using an undesirable output model. *Energies* **2020**, *13*, 26–29. doi:10.3390/en13102629.

© 2025 by the author(s). Distributed under a Creative Commons CC BY license.

Preprints.org (www.preprints.org) | NOT PEER-REVIEWED | Posted: 27 February 2026 doi:10.20944/preprints202504.2514.v4

12. Radavičius, T.; van der Heide, A.; Palitzsch, W.; Rommens, T.; Denafas, J.; Tvaronavičienė, M. Circular solar industry supply chain through product technological design changes. *Insights Reg. Dev*. **2021**, *3*, 10–30. Doi:10.9770/IRD.2021.3.3(1).hal-03583961f.
13. Akimoto, K.; Sano, F.; Oda, J.; Kanaboshi, H.; Nakano, Y. Climate change mitigation measures for global net-zero emissions and the roles of CO_2 capture and utilization and direct air capture. *Energy Clim. Change*. **2021**, *2*, 100057. Doi:10.1016/j.egycc.2021.100057.
14. Yoro, K. O.; Daramola M. O.; Sekoai P. T.; Wilson U. N.; Eterigho-Ikelegbe, O. Update on current approaches, challenges, and prospects of modeling and simulation in renewable and sustainable energy systems. *Renew Sustain Energy Rev*. **2021,** *150*, 111506. Doi:10.1016/j.rser.2021.111506.
15. Ishiguri, S. Generating renewable energy based on the circuit approach. Preprints; **2023**. Available from: https://doi.org/10.20944/preprints202306.1127.v1.
16. Ishiguri, S. Generating renewable energy based on a circuit approach (part 2) [Internet]. Preprints; **2024**. Available from: https://doi.org/10.20944/preprints202408.1690.v1.
17. Giani, A.; Eldredge Z. Quantum computing opportunities in renewable energy. *SN Comput. Sci*. **2021**, *2*, 393. Doi: 10.1007/s42979-021-00786-3.
18. Koide, S. *Quantum Theory, p.3*. Shokabo, Tokyo. 1997.
19. Matsui, N. *Electrical Equipment, p.8*. Morikita-Shuppan, Tokyo. 2000

Disclaimer/Publisher's Note: The statements, opinions and data contained in all publications are solely those of the individual author(s) and contributor(s) and not of MDPI and/or the editor(s). MDPI and/or the editor(s) disclaim responsibility for any injury to people or property resulting from any ideas, methods, instructions or products referred to in the content.

© 2025 by the author(s). Distributed under a Creative Commons CC BY license.